

# GdDO3NI, a nitroimidazole-based $T_1$ MRI contrast agent for imaging tumor hypoxia in vivo

Praveen K. Gulaka · Federico Rojas-Quijano ·  
Zoltan Kovacs · Ralph P. Mason · A. Dean Sherry ·  
Vikram D. Kodibagkar

Received: 1 July 2013 / Accepted: 28 October 2013 / Published online: 27 November 2013  
© SBIC 2013

**Abstract** Tumor hypoxia is known to affect sensitivity to radiotherapy and promote development of metastases; therefore, the ability to image tumor hypoxia in vivo could provide useful prognostic information and help tailor therapy. We previously demonstrated in vitro evidence for selective accumulation of a gadolinium tetraazacyclododecanetetraacetic acid monoamide conjugate of 2-nitroimidazole (GdDO3NI), a magnetic resonance imaging  $T_1$ -shortening agent, in hypoxic cells grown in tissue culture. We now report evidence for accumulation of GdDO3NI in hypoxic tumor tissue in vivo. Our data show that GdDO3NI accumulated significantly ( $p < 0.05$ ) in the central, poorly perfused regions of rat prostate adenocarcinoma AT1 tumors (threefold higher concentration than for the control agent) and showed better clearance from well-perfused regions and complete clearance from the surrounding muscle tissue. Inductively coupled plasma mass

spectroscopy confirmed that more GdDO3NI than control agent was retained in the central region and that more GdDO3NI was retained in the central region than at the periphery. These results show the utility of GdDO3NI to image tumor hypoxia and highlight the potential of GdDO3NI for application to image-guided interventions for radiation therapy or hypoxia-activated chemotherapy.

**Keywords** Magnetic resonance imaging · Hypoxia · Nitroimidazole · Prostate tumors

## Abbreviations

DOTA	Tetraazacyclododecanetetraacetic acid
GdDO3ABA	Gadolinium tetraazacyclododecanetetraacetic acid ( <i>n</i> -butyl)monoamide
GdDO3NI	Gadolinium tetraazacyclododecanetetraacetic acid monoamide conjugate of 2-nitroimidazole
GdDTPA	Gadolinium diethylenetriaminepentaacetic acid
GdHPDO3A	Gadolinium 10-(2-hydroxypropyl)-1,4,7-tetraazacyclododecane-1,4,7-triacetic acid
ICP-MS	Inductively coupled plasma mass spectrometry
MR	Magnetic resonance
MRI	Magnetic resonance imaging
PET	Positron emission tomography

Responsible Editor: Valerie C. Pierre.

**Electronic supplementary material** The online version of this article (doi:10.1007/s00775-013-1058-5) contains supplementary material, which is available to authorized users.

P. K. Gulaka · R. P. Mason · A. D. Sherry  
Department of Radiology, University of Texas Southwestern  
Medical Center, Dallas, TX 75390, USA

## Present Address:

P. K. Gulaka  
Samsung Electronics, Suwon, South Korea

F. Rojas-Quijano · Z. Kovacs · A. D. Sherry  
Advanced Imaging Research Center, University of Texas  
Southwestern Medical Center, Dallas, TX 75390, USA

V. D. Kodibagkar (✉)  
School of Biological and Health Systems Engineering, Arizona  
State University, Phoenix, AZ 85287-9709, USA  
e-mail: vikram.kodibagkar@asu.edu

## Introduction

Oxygen is essential for tissue health and survival. It is also an important variable in the treatment of many medical

conditions, including tumors, peripheral vascular disease, and stroke. Hypoxia is known to affect the radiation sensitivity of tumors and promote development of metastases [1]. Further, the extent of hypoxia can differ greatly in radiographically similar tumors in many cases [2]. Therefore, the ability to image hypoxia *in vivo* on an individual basis could not only provide useful prognostic information but could also be useful for developing hypoxia-targeted therapeutic approaches [1, 3]. Given the advent of novel, hypoxia-targeted therapies in various stages of development [4–6], the ability to stratify patients on the basis of the extent of tumor hypoxia could be crucial.

Tissue oxygenation status can be assessed in *ex vivo* tissue samples or *in vivo* using a variety of approaches (both invasive and noninvasive). *Ex vivo* methods of assessing hypoxia in tissues include immunohistochemical staining for intrinsic markers of hypoxia (e.g., carbonic anhydrase IX and hypoxia-inducible factor 1) [7] as well as for adducts of exogenously administered nitroimidazoles [8]. Invasive techniques include polarographic needle electrodes or fiber-optic fluorescence-based probes [9] to obtain quantitative measurements of partial pressure of oxygen in tissue, but these are limited to tumors that are readily accessible [10, 11]. As reviewed recently [11, 12], noninvasive hypoxia imaging approaches can be broadly classified into non-magnetic resonance (MR)-based and MR-based techniques; some are in the preclinical development stage and others are in use clinically. Non-MR-based methods include fluorescence imaging [13], phosphorescence quenching [14], near-infrared spectroscopy [15], single photon emission computed tomography [16], and positron emission tomography (PET) [17]. MR-based methods include blood-oxygen-level-dependent imaging [18], electron paramagnetic resonance oximetry [19], fluorocarbon relaxometry using echo planar imaging for dynamic oxygen mapping [20], and proton imaging of siloxanes for mapping tissue oxygenation levels [21].

An important strategy for imaging hypoxia exploits the principle of selective enzyme-mediated reduction of the nitro group in 2-nitroimidazole-containing compounds under hypoxic conditions [22]. Although initial studies concentrated on using 2-nitroimidazole analogs to sensitize

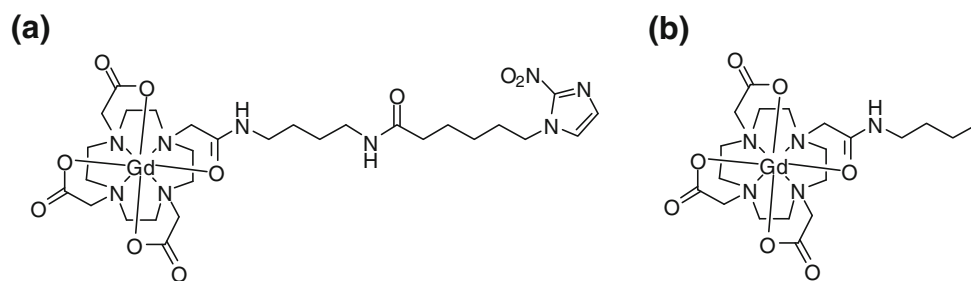
hypoxic tumors to ionizing radiation [23], soon the prospect of these compounds as potential noninvasive hypoxia-homing probes was realized, and several radiolabeled nitroimidazole derivatives have since been developed to image hypoxic tissues *in vivo* [10, 11]. Currently, [ $^{18}\text{F}$ ]fluoromisonidazole [10], [ $^{18}\text{F}$ ]fluoroazomycin-araboside [24], 2-(2-nitro-1*H*-imidazol-1-yl)-*N*-(2,2,3,3,3- $^{18}\text{F}$ pentafluoropropyl)acetamide [25], [ $^{18}\text{F}$ ]fluoroerythronitroimidazole [26], and copper-64 diacetyl-bis( $N^4$ -methylthiosemicarbazone) [27] are being evaluated as hypoxia-sensitive PET probes, and [ $^{19}\text{F}$ ]trifluoromisonidazole [28] has been used as a fluorine MR imaging (MRI) probe to qualitatively image hypoxia. Recently, we developed a gadolinium tetraazacyclododecanetetraacetic acid monoamide conjugate of 2-nitroimidazole (GdDO3NI; Fig. 1a) as a  $^1\text{H}$  MR-based hypoxia-targeting agent and showed preferential accumulation of the agent in 9L glioma cells incubated with the agent under hypoxic conditions (eightfold compared with normoxia) [29].

Since MR-based noninvasive imaging is particularly suitable for high-resolution longitudinal measurements, in this study, we investigated the potential of GdDO3NI for use as a novel hypoxia-targeting  $T_1$  MRI contrast agent. A similar structure lacking the nitroimidazole moiety, gadolinium tetraazacyclododecanetetraacetic acid (*n*-butyl)monoamide (GdDO3ABA; Fig. 1b), was used as a control [29]. Here, we compare the kinetics of GdDO3NI and GdDO3ABA uptake and washout from tumors and the tissue biodistribution of these agents after a single, bolus intravenous injection into rats bearing large, hypoxic prostate tumors.

## Materials and methods

The contrast agents GdDO3NI and GdDO3ABA (formula molecular masses 0.839 and 0.615 kDa, respectively) were synthesized as described previously [29]. All MRI studies were performed with an INOVA 4.7-T horizontal-bore MR system (Agilent Technologies, Santa Clara, CA, USA; 200 MHz for  $^1\text{H}$ ). Owing to the low molecular masses, both agents can be considered as freely diffusible small molecular agents.

**Fig. 1** Molecular structures of **a** the hypoxia-targeting magnetic resonance imaging (MRI) contrast agent GdDO3NI and **b** the control MRI contrast agent GdDO3ABA used in this study



### Spin–lattice relaxivity ( $r_1$ ) measurements

In vitro measurements of contrast agent  $T_1$  relaxivity ( $r_1$ ) were performed at 37 °C using two serial dilution phantoms (0–4 mM), one in phosphate-buffered saline and the other in 1 % agarose to simulate tissue (Fig. S1). For the relaxation rate ( $R_1$ ) measurements, a spin-echo sequence was used to acquire images at several repetition times (0.1–6 s) and a fixed echo time of 12 ms. The  $r_1$  relaxivities were determined from the slopes of the plots of the relaxation rate versus concentration.

### Kinetics of GdDO3NI versus GdDO3ABA

All the animal experiments were approved by the Institutional Animal Care and Use Committee at University of Texas Southwestern Medical Center. For in vivo studies comparing GdDO3NI with GdDO3ABA, syngeneic Dunning prostate R3327-AT1 tumors were implanted subcutaneously in ten Copenhagen rats [30]. Imaging studies were performed when the tumor sizes reached approximately 3 cm<sup>3</sup>. The anesthetized rats (1.5 % isoflurane in 1 L inhaled gas per minute) were passively restrained and the body temperature was maintained at 37 °C by a warm circulating water pad. The subcutaneous tumors growing on the leg of each rat were placed in a 3.5 cm diameter homebuilt volume coil, and multi-slice  $T_1$ -weighted images (repetition time 200 ms, echo time 10 ms, field of view 5 cm × 5 cm, matrix 128 × 128, slice thickness 1 mm) were obtained before and after injection of 0.1 mmol GdDO3NI or GdDO3ABA per kilogram body weight ( $n = 5$  each). Images were acquired every 30 s during the baseline scan and up to 3 min after injection followed by acquisition every minute up to 15 min and then once every 10 min up to 145 min after injection. The gadolinium concentration was estimated from the image data using the relationship  $C_{\text{Gd}} = (R_{1,\text{post}} - R_{1,\text{pre}})/r_1$ , where  $R_{1,\text{pre}}$  and  $R_{1,\text{post}}$  are the relaxation rates and  $r_1$  is the relaxivity of the contrast agent in a 1 % agar phantom.

### Data analysis

All data analyses were performed using MATLAB (The Mathworks, Natick, MA, USA) routines developed in-house. First, a region of interest was drawn on the  $T_2$ -weighted scout image to delineate the tumor. The percentage signal enhancement map at 90 s after injection relative to the preinjection (baseline) signal intensity was used to segment the total tumor region into well-perfused regions (enhancement at 90 s of 50 % or greater) and poorly perfused regions (enhancement at 90 s of less than 50 %). Of the voxels in the poorly perfused regions, those that showed less than 10 % enhancement at 90 min

after injection were also excluded, since they were more likely to represent necrotic regions. The well-perfused and poorly perfused regions were designated as “periphery” and “center,” respectively, as these correspond well to the empirically observed locations of most of the voxels in the well-perfused and poorly perfused regions. The statistical significance of differences in the normalized mean intensities and concentrations at each time point were estimated by using a two-tailed unpaired Student  $t$  test.

### Histology and immunohistochemistry

To confirm the presence of hypoxic tissue, tumor samples were collected for histological and immunohistochemical evaluation after staining using the hypoxia marker pimonidazole hydrochloride (Hypoxyprobe-1; Natural Pharmacia International, Belmont, MA, USA). Pimonidazole was dissolved in saline and injected via a tail vein (60 mg kg<sup>-1</sup>), and 90 min later the rats were euthanized. Tumors were excised and sections were cut through the center of the tumor. These tumor sections were then fixed in 10 % formalin and embedded in paraffin. Before hematoxylin–eosin staining and immunohistochemistry, 5 μm thick cut sections were deparaffinized in xylene and ethanol and rehydrated in water. Hypoxic regions were detected using mouse monoclonal antibody Mab1 (1:50; Natural Pharmacia International) and fluorescein isothiocyanate conjugated goat antimouse secondary antibody (1:100 dilution; Jackson ImmunoResearch Laboratories, West Grove, PA, USA). After they had been mounted with Vectashield medium (Vector Laboratories, Burlingame, CA, USA), the slides were imaged using a fluorescence microscope (DeltaVison RT, Applied Precision, Issaquah, WA, USA) equipped with a CoolSNAP<sup>HQ</sup> cooled charge-coupled device digital camera (Photometrics, Tucson, AZ, USA) with a computer-controlled motorized stepping stage. The images were reconstructed using the SoftWoRx 3.7 imaging software package (Applied Precision, Issaquah, WA, USA).

### Inductively coupled plasma mass spectroscopy

To determine the amount of retained gadolinium, inductively coupled plasma mass spectroscopy (ICP-MS) analysis of select regions of the tissue was also performed on a subset of the rats used in the imaging studies. For this, 5 mm thick tumor sections ( $n = 3$  rats) were cut and further segmented into periphery and center regions using a scalpel. These samples were then frozen immediately in liquid nitrogen and sent for ICP-MS analysis (Galbraith Laboratories, Knoxville, TN, USA). The results were compared using one-way analysis of variance followed by Tukey's multiple comparison test.

## Results

MRI reveals higher retention of GdDO3NI than GdDO3ABA in Dunning prostate R3327-AT1 tumors

The  $r_1$  relaxivity values of GdDO3NI and GdDO3ABA were determined to be  $5.21 \pm 0.04$  and  $4.74 \pm 0.03 \text{ mM}^{-1} \text{ s}^{-1}$ , respectively, in phosphate-buffered saline from imaging data collected at 4.7 T, whereas those in a tissue simulating agarose phantom (1 % w/v) were  $5.45 \pm 0.29$  and  $4.76 \pm 0.27 \text{ mM}^{-1} \text{ s}^{-1}$ , respectively (Fig. S1). The values determined in agarose were used to convert the intensities measured in vivo into the concentrations of the respective contrast agents. The kinetics of the two contrast agents were compared following intravenous injections of GdDO3NI or GdDO3ABA in Dunning prostate R3327-AT1 rat tumor bearing animals ( $n = 5$ ). The data were segmented into well-perfused and non-necrotic poorly perfused regions as described in “Data analysis” (Fig. S2). Qualitatively, the normalized time course signal intensities showed a clear difference in the enhancement patterns for the two agents (GdDO3NI and GdDO3ABA) and between peripheral and central regions (Fig. 2). In the case of GdDO3NI, hyperintense regions were observed in the center of the tumor at 145 min after injection of the contrast agent when compared with pre-injection images (Fig. 2, image c). Although some hyper-intensity was also observed in the center of the tumor in the case of GdDO3ABA, the intensities were generally much lower than with GdDO3NI (approximately 19 % over the baseline intensities, on average, for GdDO3NI vs approximately 5 % for GdDO3ABA). From comparison of the ratios of tumor to muscle intensities, a statistically significant difference ( $p < 0.05$ ) in contrast enhancement was observed between peripheral (well-perfused and consequently well oxygenated) regions and central (poorly perfused and potentially hypoxic) regions at late time points (80–145 min

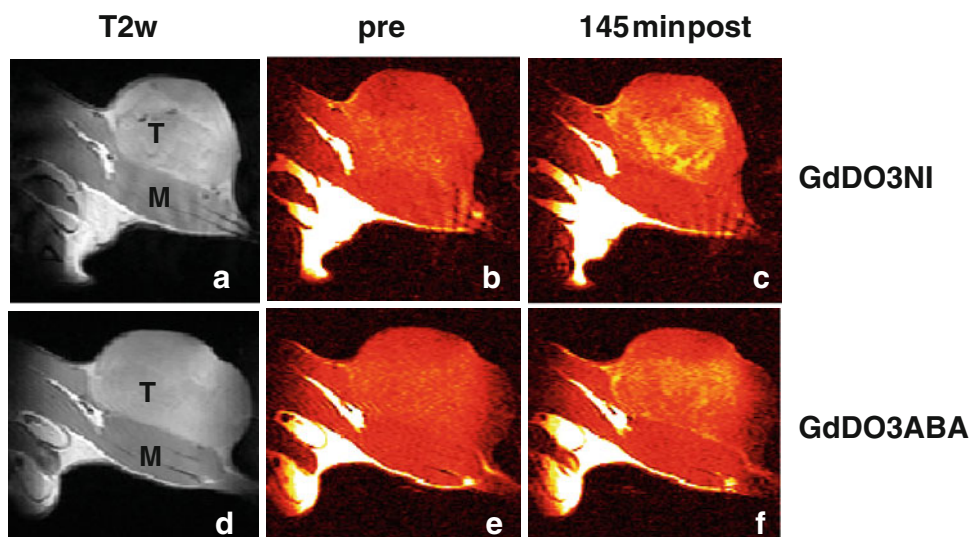
after injection) in rats given GdDO3NI (Fig. 3a), whereas for GdDO3ABA, no statistically significant difference between these regions was observed at late time points (Fig. 3b). Both agents showed a statistically significant difference in the two regions at early time points as well (up to 8 min after injection for GdDO3ABA and up to 15 min after injection for GdDO3NI).

Quantitative comparison of the time course of the gadolinium concentration obtained by MRI showed a statistically significant difference in the gadolinium concentration at late time points (100–145 min) in the central regions of tumors between rats ( $n = 5$ ) into which GdDO3NI and GdDO3ABA had been injected (Fig. 4a). No statistically significant differences in the clearance patterns were observed in the tumor periphery (Fig. 4b) or the thigh region (Fig. 4c). At 145 min after injection, the gadolinium concentrations in the center regions of the tumor were  $16.6 \pm 4.8 \text{ }\mu\text{M}$  for GdDO3NI as compared with  $5.3 \pm 5.8 \text{ }\mu\text{M}$  for GdDO3ABA. At the same time, the periphery showed a higher concentration of GdDO3ABA than GdDO3NI (Table 1). The time to reach the peak concentration was shorter for GdDO3ABA than for GdDO3NI for all three regions analyzed (thigh muscle, tumor periphery, and tumor center). The gadolinium concentration maps created at 145 min after injection of the contrast agents clearly reveal higher uptake of GdDO3NI at foci in central regions of the tumor (Fig. S3) when compared with GdDO3ABA (Fig. S4).

Ex vivo tumor sample analysis correlates GdDO3NI retention with the presence of hypoxia in Dunning prostate R3327-AT1 tumors

Histological analysis (Fig. 5a) and pimonidazole staining and imaging by immunofluorescence (Fig. 5b) confirmed the existence of three zones in the tumor: a necrotic center surrounded by a region composed of sparse vasculature and

**Fig. 2** Grayscale magnetic resonance  $T_2$ -weighted (a, d) and color  $T_1$ -weighted (b, c, e, f) images of Copenhagen rat thighs bearing syngeneic Dunning prostate R3327-AT1 tumors following injection of 0.1 mmol GdDO3NI per kilogram body weight (a–c) or 0.1 mmol GdDO3ABA per kilogram body weight (d–f) before injection (b, e) and 145 min after injection (c, f). The tumor and thigh muscle are labeled T and M, respectively



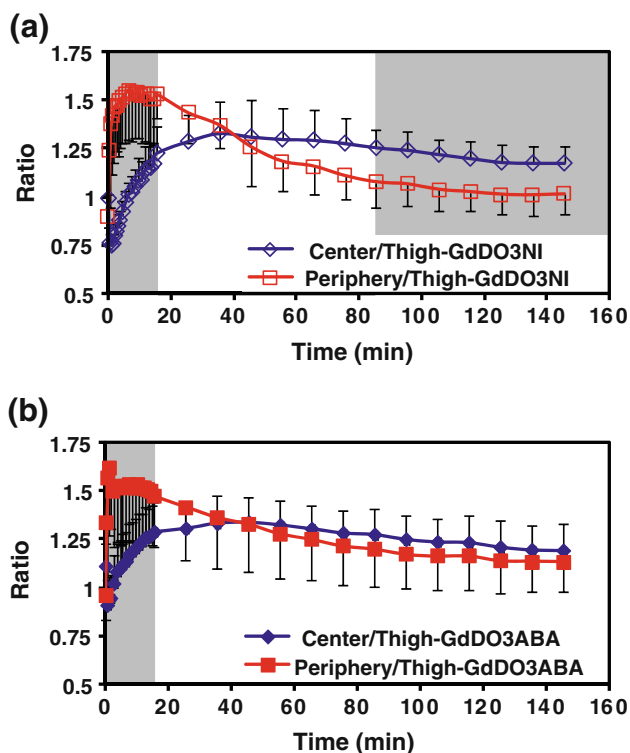


**Fig. 3** Comparison of the time course of normalized mean intensities ( $n = 5$ ) for well-perfused (periphery) and poorly perfused (center) regions of Dunning prostate R3327-AT1 tumors in rats into which **a** 0.1 mmol GdDO3NI per kilogram body weight or **b** 0.1 mmol GdDO3ABA per kilogram body weight had been injected. Normalization was performed with respect to the mean intensity in thigh muscle tissue for each rat before averaging. Regions in *gray* represent time intervals showing a statistically significant difference ( $p < 0.05$ , two-tailed unpaired  $t$  test) between the two contrast agents at each measurement time point in the interval

hypoxic regions and a viable well-perfused periphery. ICP-MS analysis of tumor sections (*ex vivo*) was performed to quantify the gadolinium concentration. The tumor sections were cut to delineate the periphery and core to mimic the MR segmentation procedure used here, following which the samples were sent for ICP-MS analysis. The concentration of gadolinium (Fig. 6) was significantly higher in the central tumor region of rats ( $n = 3$ ) into which GdDO3NI had been injected when compared with its periphery as well as tumor regions of rats ( $n = 3$ ) into which GdDO3ABA had been injected. On average, an approximately 50-fold higher retention of gadolinium was observed by ICP-MS in central regions of tumors into which GdDO3NI had been injected when compared with tumors into which GdDO3ABA had been injected.

**Discussion**

The vital role of hypoxia in the development and malignant progression in various cancers has been well

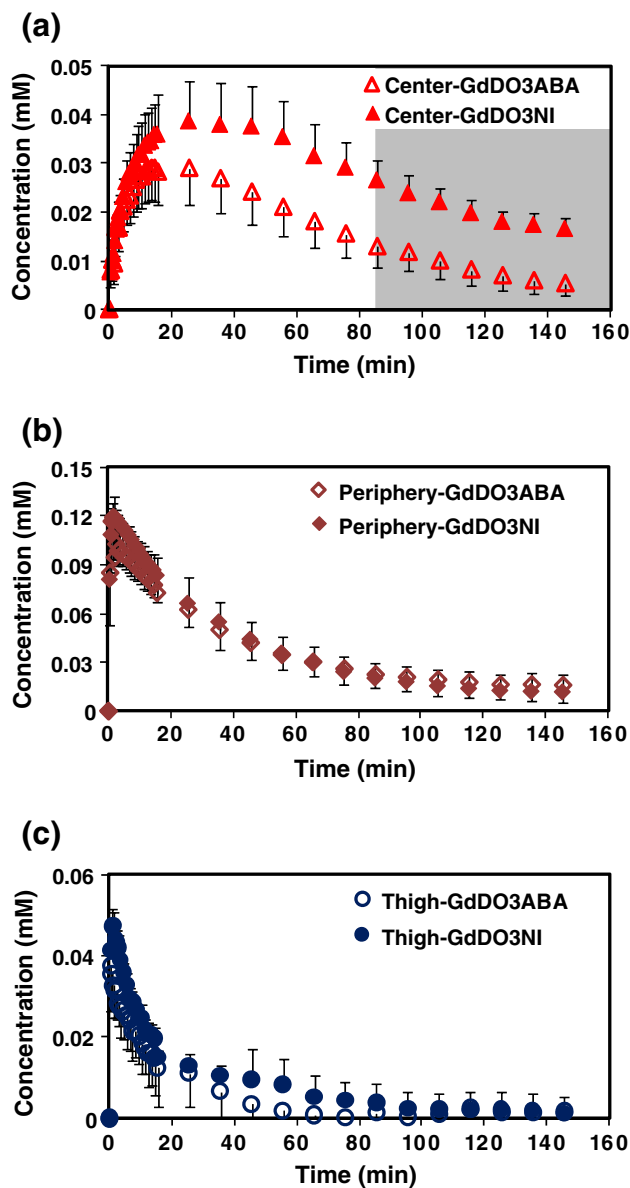


**Fig. 4** Kinetics of mean gadolinium concentration ( $n = 5$ ) for **a** poorly perfused (central) regions of tumors, **b** well-perfused (peripheral) regions of tumors, and **c** thigh muscle tissue in rats into which 0.1 mmol GdDO3NI or GdDO3ABA per kilogram body weight had been injected. Regions in *gray* represent time intervals showing a statistically significant difference ( $p < 0.05$ , two-tailed unpaired  $t$  test) between the two contrast agents at each measurement time point in the interval

studied. Hypoxia is also an important factor in determining the efficacy of radiotherapy, photodynamic therapy, and some chemotherapies, and information related to hypoxic regions could be clinically important [3]. Our study has tried to address this issue by evaluating a novel hypoxia-targeting MRI contrast agent, GdDO3NI, with respect to the following attributes: (a) being an effective reporter of hypoxia, suitable for noninvasive *in vivo* studies, and (b) making possible high-resolution

**Table 1** Contrast agent kinetic parameters determined by magnetic resonance imaging in Copenhagen rat thighs bearing syngeneic Dunning prostate R3327-AT1 tumor following injection of 0.1 mmol gadolinium tetraazacyclododecanetetraacetic acid monoamide

	GdDO3NI			GdDO3ABA		
	Time to peak (min)	Peak concentration ( $\mu\text{M}$ )	Final concentration ( $\mu\text{M}$ )	Time to peak (min)	Peak concentration ( $\mu\text{M}$ )	Final concentration ( $\mu\text{M}$ )
Thigh muscle	1.5	$48 \pm 7$	$1 \pm 10$	0.5	$38 \pm 11$	$-2 \pm 7$
Tumor periphery	2.5	$119 \pm 25$	$12 \pm 6$	1.5	$119 \pm 9$	$16 \pm 6$
Tumor center	22.5	$39 \pm 18$	$17 \pm 5$	14.5	$29 \pm 16$	$5 \pm 6$

*Time to peak* refers to the time after contrast agent injection at which the listed peak concentrations were observed. The final concentrations were measured at 145 min after injection

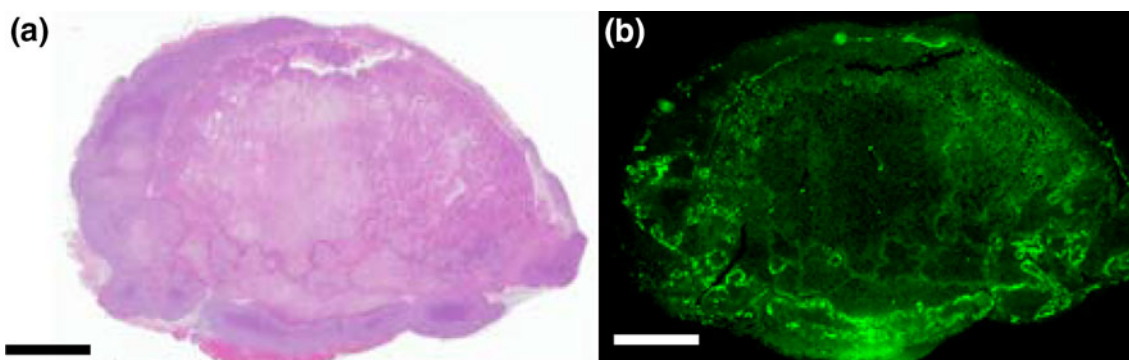


**Fig. 5** **a** Cellularity by hematoxylin–eosin staining and **b** hypoxia distribution by pimonidazole-based immunohistochemical staining in a Dunning prostate R3327-AT1 tumor section. The pimonidazole

staining clearly showed extensive hypoxia in regions of the tumor. The scale bars represent 0.5 cm

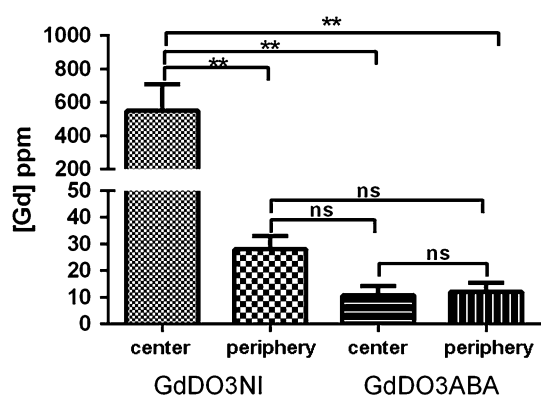


**Fig. 6** Inductively coupled plasma mass spectroscopy analysis of tumor sections ex vivo. The central or core regions of Dunning prostate R3327-AT1 tumors of rats into which 0.1 mmol GdDO3NI per kilogram body weight had been injected showed significantly enhanced retention of  $\text{Gd}^{3+}$ , clearly validating GdDO3NI as a hypoxia-targeting agent. Two asterisks represents  $p < 0.05$  following one-way analysis of variance

$^1\text{H}$  MRI to show the heterogeneity of hypoxia distribution in solid tumors.

Macrocyclic compounds and their derivatives are widely used as chelating agents in imaging probe development as

they can form highly stable chelates with lanthanide metals [31]. In addition, the coordination chemistry of these compounds has been well studied [32, 33], allowing the design of targeted probes for in vivo applications. Previously, radiolabeled lanthanide 2-nitroimidazole conjugates with DOTA derivatives were synthesized for imaging of hypoxia [34–37]. To our knowledge, our work is the first report on a 2-nitroimidazole derivative as a  $^1\text{H}$  MRI probe to detect hypoxia. GdDO3ABA was used as the “control agent” as it has a structure similar to that of GdDO3NI without the hypoxia-targeting nitroimidazole moiety. Having previously demonstrated the hypoxia-targeting ability in vitro using cells incubated under hypoxic conditions [29], we have now successfully validated the novel gadolinium-based nitroimidazole as a  $T_1$  contrast agent (GdDO3NI) for MRI of hypoxia.

Since our main objective was to evaluate the hypoxia-targeting capability of GdDO3NI, the choice of in vivo (tumor) models was of paramount importance. Another focus of this study was to determine the in vivo contrast agent kinetics as well as the ability to detect the spatial distribution of hypoxia in tumor models. Therefore, we chose large (approximately  $3\text{ cm}^3$ ) Dunning prostate R3327-AT1 tumors as they have been shown using  $^{19}\text{F}$  MR

oximetry to be extensively hypoxic (mean values of partial pressure of oxygen in tissue of  $3.5 \pm 1.5$  Torr) [30]. In future studies, spontaneous or orthotopic tumor models might be appropriate, as well, for testing therapeutic interventions based on imaging hypoxia (e.g., tumor stratification for use of hypoxia-targeting chemotherapeutics).

The observed signal intensities and derived concentrations of the agents increased fastest in the well-perfused regions of tumors because of rapid contrast agent influx (Fig. 4b). This was followed by fast washout, irrespective of the contrast agent (GdDO3NI or GdDO3ABA). In contrast, central regions, typically characterized by deficits in vascular supply, showed a delay in signal buildup corresponding to a delayed uptake for both contrast agents (Fig. 4a), as also reported for this tumor type previously for gadolinium diethylenetriaminepentaacetic acid (GdDTPA) [38]. More GdDO3NI than GdDO3ABA was retained in the central regions at late time points and we attribute this retention to the presence of hypoxia-activated binding of GdDO3NI. The wash-in kinetics were different for both contrast agents (Table 1), with increased time to peak intensities in all regions for GdDO3NI compared with GdDO3ABA. This is consistent with the expected kinetics for a targeted agent versus an untargeted one [39]. GdDO3NI and GdDO3ABA were also observed in the peripheral regions. In general, the tumor vasculature, even in the well-perfused region, is chaotic and poorly functional [40], and regions of hypoxia can coexist with vasculature within the volume of an MRI voxel ( $390 \mu\text{m} \times 390 \mu\text{m} \times 1,000 \mu\text{m}$  in this case). Similarly, agents that are nonspecific for hypoxia also accumulate in hypoxic or necrotic regions by passive diffusion and demonstrate enhanced retention [41]. Indeed, GdDTPA (a non-hypoxia-specific clinical contrast agent) based pharmacokinetic parameters have been shown to correlate with hypoxia [42]. Fitting a first-order-decaying exponential function of the form  $C = C_0 + A_{\text{exp}}(-t/t_1)$  to the late time concentration time course (85–145 min) yields a residual concentration  $C_0$  of  $13 \pm 2 \mu\text{M}$  in the central region for GdDO3NI compared with  $-2 \pm 4 \mu\text{M}$ , i.e., complete clearance, for GdDO3ABA. Thus, the combination of differential kinetics and retention at late time points adds confidence to hypoxia-specific retention in the central regions of the tumor. Pimonidazole staining of the excised AT1 tumor tissues confirmed the presence of extensive hypoxia throughout the central regions of the tumor (Fig. 5b). Also, ICP-MS analysis of the AT1 tumor samples revalidated the presence of excess amounts of gadolinium in the central regions of rats into which GdDO3NI had been injected (Fig. 6) as observed from the concentration maps (Fig. 4a, Table 1). Interestingly, the amount of GdDO3NI found by ICP-MS in the central tumor region (549 ppm, equivalent to 549  $\mu\text{g}$  Gd per gram of tissue)

was significantly higher than that estimated by MRI using a presumed intracellular relaxivity equal to that measured in 1 % agarose. If one assumes that 1 g of tissue contains approximately 0.6 mL of water, then the concentration of gadolinium in this region could be as high as 5.84 mM. This is approximately 365-fold higher than the concentration estimated by MRI (16  $\mu\text{M}$ ). If anything, one would expect that  $r_1$  of the agent would be higher when it is bound to a larger macromolecular structure inside the cell, so the MRI estimate of 16  $\mu\text{M}$  would be an upper limit if the agent has full access to water. This surprising result suggests that much of the GdDO3NI trapped in hypoxic cells does not have full access to water, i.e., it has a much lower relaxivity than that measured for the complex in aqueous media, such that MRI underestimates the true amount of GdDO3NI in cells. This is entirely consistent with a previous study by Terreno et al. [43], who showed that the relaxivity of gadolinium 10-(2-hydroxypropyl)-1,4,7-tetraazacyclododecane-1,4,7-triacetic acid (GdHPDO3A) when loaded into cells by electroporation versus pinocytosis differs considerably. These differences in relaxivity were ascribed to differences in the intracellular location of the contrast agent (cytoplasm using electroporation versus endosomal vesicles using pinocytosis). This same group later showed by using photochemical release of endosomal GdHPDO3A molecules entrapped by pinocytosis that the relaxivity of the contrast agent increased considerably as it moved into the cytoplasm [44]. Further modeling of the data suggested that the difference in proton relaxation rates between the cytoplasmic and the extracellular compartment is higher than the exchange rate of water molecules across the cellular membrane. Given the current uncertainty in the intracellular location and chemical environment of GdDO3NI when trapped in hypoxic cells, it is not unreasonable to assume that the contrast agent is confined to a space within cells that has limited water access or where water exchange between that environment and extracellular water is slow. On the basis of the tissue concentration of GdDO3NI estimated by ICP-MS, one can estimate that the effective  $r_1$  relaxivity of the trapped contrast agent is only  $0.015 \text{ mM}^{-1} \text{ s}^{-1}$ . In any case, the injected dose used in this study (0.1 mmol per kilogram body weight) corresponds to a typical dose of GdDTPA used in the clinic and was sufficient to clearly highlight regions of hypoxia (Fig. 2).

An important parameter for imaging is the acquisition resolution. Irrespective of the imaging technique or modality, every value that is obtained is an ensemble average of the microscopic variations present in the measured voxel. The current clinical hypoxia imaging resolution reported using PET of [ $^{18}\text{F}$ ]fluoromisonidazole is approximately  $5 \text{ mm} \times 5 \text{ mm}$ , whereas the new

preclinical PET scanners can achieve a resolution of 1 mm × 1 mm [45]. Our data, using the contrast agent GdDO3NI, were acquired at anatomical <sup>1</sup>H MRI resolution of 390 μm × 390 μm, which is achievable with clinical MRI scanners. We were limited by temporal resolution (30 s at early time points) in our selection of the acquisition resolution; even higher resolution would have been possible for imaging a single time point.

In this study, GdDO3NI was shown to reveal hypoxia at anatomical MRI resolution with standard dosing. Since MRI is non-invasive, this contrast agent also has the potential for imaging modulation of tumor hypoxia by hyperoxic or hypoxic interventions. It could also help us better understand treatment-induced changes in tumor oxygenation, particularly hypoxia-targeting therapy. This capability could have profound implications for cancer treatment as it is practiced today and could lead to more personalized therapeutic decisions. Further evaluation of the targeting efficiency of GdDO3NI at different levels of hypoxia as well as subcellular localization, *in vitro*, will help in better understanding the mechanism and quantification of data, potentially leading to quantitative oximetry. Given the preliminary results reported here, a further one-to-one comparison study using PET in the preclinical setting would be beneficial in providing further support of the clinical translation potential of MRI hypoxia reporters such as GdDO3NI. The development of an appropriate theoretical model for contrast kinetics of an MRI-based hypoxia targeting agent that takes into account the arterial input function would be critical for quantitative analysis of the data. To the best of our knowledge, such a model has not been published to date and it will be a focus of our efforts in the near future.

**Acknowledgments** This research was supported in part by grants from the Norman Hackerman ARP grant (010019-0056-2007), the National Institutes of Health (R21CA132096, R01CA139043 and R01CA115531), the Southwestern Small Animal Imaging Research Program (U24 CA126608), and the Robert A. Welch Foundation (AT-584). MRI experiments were performed at the Advanced Imaging Research Center with support from a National Institutes of Health National Institute of Biomedical Imaging and Bioengineering resource grant (P41EB015908). We would like to thank Li Liu and Abhijit Bugde for helpful advice.

## References

- Tatum JL, Kelloff GJ, Gillies RJ, Arbeit JM, Brown JM, Chao KS, Chapman JD, Eckelman WC, Fyles AW, Giaccia AJ, Hill RP, Koch CJ, Krishna MC, Krohn KA, Lewis JS, Mason RP, Melillo G, Padhani AR, Powis G, Rajendran JG, Reba R, Robinson SP, Semenza GL, Swartz HM, Vaupel P, Yang D, Croft B, Hoffman J, Liu G, Stone H, Sullivan D (2006) *Int J Radiat Biol* 82:699–757
- Hockel M, Vaupel P (2001) *J Natl Cancer Inst* 93:266–276
- Vaupel P, Mayer A (2007) *Cancer Metastasis Rev* 26:225–239
- Liu Q, Sun JD, Wang J, Ahluwalia D, Baker AF, Cranmer LD, Ferraro D, Wang Y, Duan JX, Ammons WS, Curd JG, Matteucci MD, Hart CP (2012) *Cancer Chemother Pharmacol* 69:1487–1498
- McKeage MJ, Jameson MB, Ramanathan RK, Rajendran J, Gu Y, Wilson WR, Melink TJ, Tchekmedyan NS (2012) *BMC Cancer* 12:496
- Le QT, Fisher R, Oliner KS, Young RJ, Cao H, Kong C, Graves E, Hicks RJ, McArthur GA, Peters L, O'Sullivan B, Giaccia A, Rischin D (2012) *Clin Cancer Res* 18:1798–1807
- He F, Deng X, Wen B, Liu Y, Sun X, Xing L, Minami A, Huang Y, Chen Q, Zanzonico PB, Ling CC, Li GC (2008) *Cancer Res* 68:8597–8606
- Russell J, Carlin S, Burke SA, Wen B, Yang KM, Ling CC (2009) *Int J Radiat Oncol Biol Phys* 73:1177–1186
- Griffiths JR, Robinson SP (1999) *Br J Radiol* 72:627–630
- Krohn KA, Link JM, Mason RP (2008) *J Nucl Med* 49(Suppl 2):129S–148S
- Mason RP, Zhao D, Pacheco-Torres J, Cui W, Kodibagkar VD, Gulaka PK, Hao G, Thorpe P, Hahn EW, Peschke P (2010) *Q J Nucl Med Mol Imaging* 54:259–280
- Zhao D, Jiang L, Mason RP (2004) *Methods Enzymol* 386:378–418
- Takahashi E, Takano T, Nomura Y, Okano S, Nakajima O, Sato M (2006) *Am J Physiol Cell Physiol* 291:C781–C787
- Bussink J, Kaanders JH, Strik AM, Vojnovic B, van der Kogel AJ (2000) *Radiat Res* 154:547–555
- Xia M, Kodibagkar V, Liu H, Mason RP (2006) *Phys Med Biol* 51:45–60
- Li L, Yu JM, Xing LG, Yang GR, Sun XD, Xu J, Zhu H, Yue JB (2006) *Chin Med J (Engl)* 119:1477–1480
- Lewis JS, McCarthy DW, McCarthy TJ, Fujibayashi Y, Welch MJ (1999) *J Nucl Med* 40:177–183
- Baudelet C, Gallez B (2002) *Magn Reson Med* 48:980–986
- Gallez B, Baudelet C, Jordan BF (2004) *NMR Biomed* 17:240–262
- Hunjan S, Zhao D, Constantinescu A, Hahn EW, Antich PP, Mason RP (2001) *Int J Radiat Oncol Biol Phys* 49:1097–1108
- Kodibagkar VD, Wang X, Pacheco-Torres J, Gulaka P, Mason RP (2008) *NMR Biomed* 21:899–907
- Kedderis GL, Miwa GT (1988) *Drug Metab Rev* 19:33–62
- Brown JM (1975) *Radiat Res* 64:633–647
- Piert M, Machulla HJ, Picchio M, Reischl G, Ziegler S, Kumar P, Wester HJ, Beck R, McEwan AJ, Wiebe LI, Schwaiger M (2005) *J Nucl Med* 46:106–113
- Evans SM, Kachur AV, Shiue CY, Hustinx R, Jenkins WT, Shive GG, Karp JS, Alavi A, Lord EM, Dolbier WR Jr, Koch CJ (2000) *J Nucl Med* 41:327–336
- Yang DJ, Wallace S, Cherif A, Li C, Gretzer MB, Kim EE, Podoloff DA (1995) *Radiology* 194:795–800
- Lewis J, Laforest R, Buettner T, Song S, Fujibayashi Y, Connert J, Welch M (2001) *Proc Natl Acad Sci USA* 98:1206–1211
- Procissi D, Claus F, Burgman P, Koziorowski J, Chapman JD, Thakur SB, Matei C, Ling CC, Koutcher JA (2007) *Clin Cancer Res* 13:3738–3747
- Rojas-Quijano FA, Tircso G, Tircsone Benyo E, Baranyai Z, Tran Hoang H, Kalman FK, Gulaka PK, Kodibagkar VD, Aime S, Kovacs Z, Sherry AD (2012) *Chemistry* 18:9669–9676
- Zhao D, Ran S, Constantinescu A, Hahn EW, Mason RP (2003) *Neoplasia* 5:308–318
- Aime S, Crich SG, Gianolio E, Giovenzana GB, Tei L, Terreno E (2006) *Coord Chem Rev* 250:1562–1579
- Sherry AD, Brown RD, Gerales CFG, Koenig SH, Kuan KT, Spiller M (1989) *Inorg Chem* 28:620–622
- Aime S, Anelli PL, Botta M, Fedeli F, Grandi M, Paoli P, Uggeri F (1992) *Inorg Chem* 31:2422–2428



34. Norman TJ, Smith FC, Parker D, Harrison A, Royle L, Walker CA (1995) *Supramol Chem* 4:305–308
35. Das T, Chakraborty S, Banerjee S, Mukherjee A, Samuel G, Sarma HD, Nair CK, Kagiya VT, Venkatesh M (2004) *Bioorg Med Chem* 12:6077–6084
36. Hoigebazar L, Jeong JM, Choi SY, Choi JY, Shetty D, Lee YS, Lee DS, Chung JK, Lee MC, Chung YK (2010) *J Med Chem* 53:6378–6385
37. Hoigebazar L, Jeong JM, Hong MK, Kim YJ, Lee JY, Shetty D, Lee YS, Lee DS, Chung JK, Lee MC (2011) *Bioorg Med Chem* 19:2176–2181
38. Jiang L, Zhao D, Constantinescu A, Mason RP (2004) *Magn Reson Med* 51:953–960
39. Davis SC, Samkoe KS, Tichauer KM, Sexton KJ, Gunn JR, Deharvengt SJ, Hasan T, Pogue BW (2013) *Proc Natl Acad Sci USA* 110:9025–9030
40. Vaupel P, Kallinowski F, Okunieff P (1989) *Cancer Res* 49:6449–6465
41. Fluckiger JU, Loveless ME, Barnes SL, Lepage M, Yankeelov TE (2013) *Phys Med Biol* 58:1983–1998
42. Egeland TA, Gulliksrud K, Gaustad JV, Mathiesen B, Rofstad EK (2012) *Magn Reson Med* 67:519–530
43. Terreno E, Geninatti C, Belfiore S, Biancone L, Cabella C, Esposito G, Manazza AD, Aime S (2006) *Magn Reson Med* 55:491–497
44. Gianolio E, Arena F, Strijkers GJ, Nicolay K, Högset A, Aime S (2011) *Magn Reson Med* 65:212–219
45. Cho H, Ackerstaff E, Carlin S, Lupu ME, Wang Y, Rizwan A, O'Donoghue J, Ling CC, Humm JL, Zanzonico PB, Koutcher JA (2009) *Neoplasia* 11:247–259